15th Australasian Fluid Mechanics Conference
The University of Sydney, Sydney, Australia
13-17 December 2004

Three-Dimensional Instabilities and Transition in Pulsatile Stenotic Flows

H. M. Blackburn[1] **and S. J. Sherwin**[2]

[1]CSIRO Manufacturing and Infrastructure Technology,
Highett, Vic., 3190, AUSTRALIA

[2]Department of Aeronautics, Imperial College London,
South Kensington Campus, London, SW7 2AZ, UK

Abstract

A straight tube with a smooth axisymmetric constriction is an idealised representation of a stenosed artery. We examine the three-dimensional instability of steady flow plus an oscillatory component in a tube with a smooth 75% stenosis using both linear stability analysis and direct numerical simulation. These flows become unstable through a subcritical period-doubling bifurcation involving alternating tilting of the vortex rings that are ejected from the throat with each pulse. These tilted vortex rings rapidly break down through a self-induction mechanism within the confines of the tube. While the linear instability modes for pulsatile flow have maximum energy well downstream of the stenosis, we have established using direct numerical simulation that breakdown can gradually propagate upstream until it occurs within a few tube diameters of the constriction, in agreement with previous experimental observations.

Introduction

Atherosclerosis, the formation of plaques within the arterial wall, continues to be a major cause of death in the developed world. The associated narrowing, or stenosis, of the artery can lead to potential significant restriction of blood flow to downstream vessels. Related to this condition is the potential of plaque ruptures and thrombosis formation leading to particles becoming lodged in smaller vessels possibly inducing myocardinal infarction or stroke.

This association of arterial disease with flow related mechanisms, such as wall shear stress variation, has motivated the study of steady and pulsatile flow within both idealised axisymmetric and anatomically correct arterial model stenoses [4]. Under standard physiological flow conditions most arterial flows are usually considered to be laminar, although typically separated and unsteady. However in the case of a stenotic flow the increase in local Reynolds number at a contraction can lead to transitional flow associated with the early stages of turbulence. The occurrence of turbulence-like flow phenomena makes the numerical simulation of these flows particularly challenging especially when considering the large range of parameters required to describe both the geometrical and flow features.

In the current work, we turn our attention to the stability of pulsatile flows in an axisymmetric stenotic tube. The approach adopted is to analyse the global linear stability of the axisymmetric flows to arbitrary three-dimensional perturbations. As the problem has rotational symmetry about the cylindrical axis, it is natural to use Fourier decomposition in the azimuth direction in order to break the general three-dimensional linear stability problem into a set of two-dimensional ones, dramatically reducing the size of each individual problem. Once we have the most unstable mode, we then use full three-dimensional direct numerical simulation (DNS) in order to examine the evolution of their instability modes, onset of turbulence, and nonlinear dynamics.

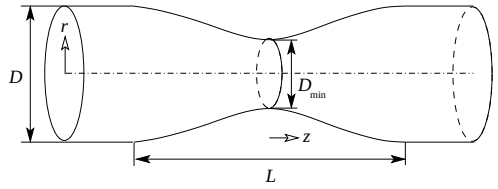

Figure 1: Geometrical parameters that define the axisymmetric sinusoidal stenosis.

Parameter Space

We will take our length scale D as the tube diameter and base the Reynolds number on the temporally and spatially averaged inflow velocity $\bar{u}$. The axisymmetric stenosis shown in figure 1 is described by a sinusoidal shape which can be described by two geometric parameters: the stenosis degree $S = 1 - (D_{\min}/D)^2$ and the stenosis length $\lambda = L/D$. We have considered the geometry defined by $S = 0.75$ and $\lambda = 2$.

To complement the geometric factors we also need to consider the physiological flow parameters. If we permit the inflow to have a pulsatile waveform of period T and restrict attention to cases of non-reversing, spatially averaged flow we can identify three important flow parameters: the Reynolds number, *Re*; the Womersley number, $\alpha = (D^2\pi/(2\nu T))^{1/2}$ and the peak to mean flow ratio $U_{pm} = Q_{\text{peak}}/Q_{\text{mean}}$, where Q is the volume flux. The Womersley number can be interpreted as the ratio of the diameter (or radius) to the viscous boundary layer growth in time period T which is the ratio of two sectional length scales. An alternative parameter commonly used in fluid mechanics is the reduced velocity $U_{red} = \bar{u}T/D$ which is the ratio of the convective length the mean flow moves in time T to the diameter. For geometries where there is a length scale in the flow direction, as is the case of the stenosis, this non-dimensional parameter can prove to be a useful alternative to the Womersley number. We note that U_{red} and α are dependent parameters related by the Reynolds number according to $U_{red} = \pi Re/(2\alpha^2)$.

Governing Equations

We consider the flow to be governed by the incompressible Newtonian Navier–Stokes equations

$$\partial_t \mathbf{u} = -\mathbf{A}(\mathbf{u}) - \nabla P + \nu\nabla^2\mathbf{u}, \quad \text{with} \quad \nabla\cdot\mathbf{u} = 0, \qquad (1)$$

where $\mathbf{u} = \mathbf{u}(z,r,\theta,t) = (u,v,w)(t)$ is the velocity field, $\mathbf{A}(\mathbf{u})$ represents nonlinear advection terms, $P = p/\rho$, and where p is the pressure, ρ and ν are respectively the fluid density and ν kinematic viscosity. The variables z, r, θ and t are respectively the axial, radial, azimuthal and time coordinates and u, v, w the velocity components in the axial, radial and azimuthal directions. We can consider the nonlinear terms either in convective form $\mathbf{A}(\mathbf{u}) = \mathbf{u}\cdot\nabla\mathbf{u}$, conservative form $\mathbf{A}(\mathbf{u}) = \nabla\cdot\mathbf{uu}$, or skew-symmetric form $\mathbf{A}(\mathbf{u}) = (\mathbf{u}\cdot\nabla\mathbf{u} + \nabla\cdot\mathbf{uu})/2$, which are

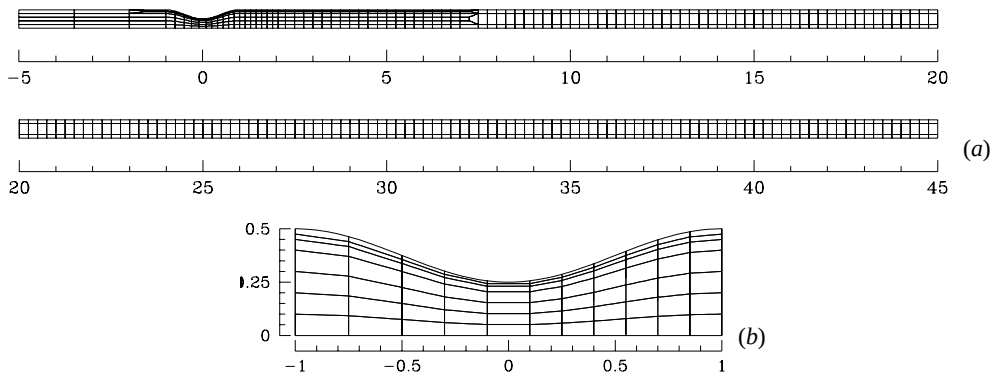

Figure 2: Spectral element outlines of computational mesh, dimensions given in terms of tube diameter D. Panel (*a*) shows elements for the first mesh with an outflow at $45D$. Panel (*b*) shows a close-up of the throat, with curved element edges.

all equivalent in a continuum setting. Equation (1) is subject to no-slip boundary conditions at the walls, a prescribed velocity at the inflow (steady or periodic), conditions of zero pressure and zero outward normal derivatives of velocity at the outflow and consistent regularity boundary conditions at the axis as explained in [7].

Taking the pressure to represent the solution of a Poisson equation that has the divergence of the advection terms as forcing, we can consider the Navier–Stokes equations in symbolic form as

$$\partial_t \mathbf{u} = -(\mathbf{I} - \nabla\nabla^{-2}\nabla\cdot)\mathbf{A}(\mathbf{u}) + \nu\nabla^2\mathbf{u} = \mathbf{N}(\mathbf{u}) + \mathbf{L}(\mathbf{u}) \qquad (2)$$

where the nonlinear operator $\mathbf{N}$ contains contributions from both pressure and advection terms, while the linear operator $\mathbf{L}$ corresponds to viscous diffusion.

When analysing the linear stability of a flow in terms of its normal modes, we decompose the velocity $\mathbf{u}$ into a base flow $\mathbf{U}$ and perturbation flow $\mathbf{u}'$: $\mathbf{u} = \mathbf{U} + \mathbf{u}'$, and examine the stability of the perturbation linearised about the base flow. In this decomposition, the original nonlinear advection terms are replaced with their linearised equivalent (here for the convective form) $\partial_{\mathbf{U}}\mathbf{A}(\mathbf{u}') = \mathbf{U}\cdot\nabla\mathbf{u}' + \mathbf{u}'\cdot\nabla\mathbf{U}$ and in symbolic form we write

$$\partial_t \mathbf{u}' = \partial_{\mathbf{U}}\mathbf{N}(\mathbf{u}') + \mathbf{L}(\mathbf{u}') \qquad (3)$$

for the evolution of the linear perturbation. If the base flow is T-periodic in time, $\partial_{\mathbf{U}}\mathbf{N}$ is linear time-periodic, and

$$\mathbf{u}'(t_0 + T) = \exp\left[\int_{t_0}^{t_0+T} (\partial_{\mathbf{U}}\mathbf{N} + \mathbf{L})\,\mathrm{d}t\right]\mathbf{u}'(t_0). \qquad (4)$$

The eigenpairs of this Floquet problem are $\{\mu,\ \tilde{\mathbf{u}}(t_0)\}$ where μ is a Floquet multiplier and $\tilde{\mathbf{u}}(t_0)$ is the T-periodic Floquet eigenfunction, evaluated at phase t_0. The equivalent to the eigenvalues γ of the time-invariant case are the Floquet exponents σ, related to the multipliers by $\mu = \exp\sigma T$. In general, the Floquet multipliers/exponents and eigenfunctions occur in complex-conjugate pairs.

Since the geometry is axisymmetric, the velocity must be 2π-periodic in θ and can be projected exactly onto a set of two-dimensional complex Fourier modes by

$$\hat{\mathbf{u}}_k(z,r,t) = \frac{1}{2\pi}\int_0^{2\pi} \mathbf{u}(z,r,\theta,t)\exp(-\mathrm{i}k\theta)\,\mathrm{d}\theta \qquad (5)$$

where k is an integer wavenumber. The Fourier-transformed equations of motion and axial boundary conditions for the velocity and pressure (and their perturbations) in cylindrical coordinates are described in detail in [5, 7]. Our base flows are both axisymmetric/two-dimensional, i.e. $\widehat{\mathbf{U}}_k = \mathbf{0}$, $k \neq 0$, and two-component, i.e. $\mathbf{U} \equiv (U,V,0)$. In the numerical stability analysis we take advantage of linearity, which decouples the stability problem for each $\hat{\mathbf{u}}'_k$.

Numerical Methods

For time evolution of both the full and linearised Navier–Stokes equations, we relied on standard (nodal-Gauss–Lobatto–Legendre) spectral elements in (z, r) and Fourier expansions if required in the azimuthal θ-direction. This spatial discretisation was coupled with a second-order-time velocity correction time-integration scheme. The development of this numerical method for DNS has been described in detail in [7]. The application of the method to linearised Navier–Stokes evolution, including appropriate boundary conditions, has also previously been described in [5].

The computational mesh used in the calculations is shown in figure 2. The domain consists of 743 elemental regions. In each element, two-dimensional mapped tensor-product Lagrange-interpolant shape functions based on the Gauss–Lobatto–Legendre nodes were applied. At $P = 7$ this elemental discretisation corresponds to approximately 38 000 local degrees of freedom in each meridional semiplane. The domain extended $5D$ upstream and $45D$ downstream of the throat. As shown in figure 2 (*b*) a fine radial mesh spacing was adopted in the region of the stenosis where two layers each of 5% of the local radius were applied. At $z/D \approx 7$ the radial mesh spacing was coarsened to allow a uniform axial spacing of $0.5D$ to be applied to the outflow. The mesh was refined until both the axisymmetric base flows and Floquet multipliers converged to four significant figures. Typically this also gives enough mesh refinement in the meridional semi-plane for non-axisymmetric DNS as well, with the number of planes of data in azimuth selected to provide a three-order or better reduction in kinetic energy from azimuthal mode 1 to the highest mode.

The numerical methods employed for stability analysis of both steady and pulsatile flow follow those outlined in [10], and previously described and used in other works [3, 5, 6]. The analysis is based on a Krylov-subspace iteration of successive finite increments of (initially random) perturbations through the operator of (4) using an Arnoldi method to extract the dominant eigenpairs of the exponential operators in the equations. The data used to supply the T-periodic base flow are approximated through Fourier-series reconstruction from a limited number (typically 256) of time-slices obtained from two-dimensional DNS.

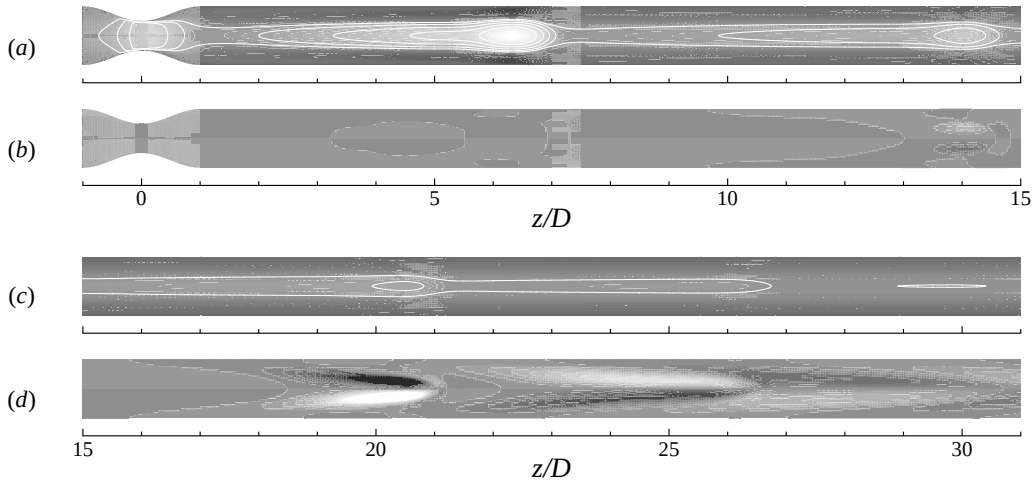

Figure 3: The base flow and the leading eigenmode for one phase in the flow cycle for the unstable pulsatile flow at $Re = 400$, $U_{red} = 2.5$, on a vertical centreplane. Panels (*a*, *c*) show contours of axial velocity of the base flow, while (*b*, *d*) show contours of axial velocity of the eigenmode.

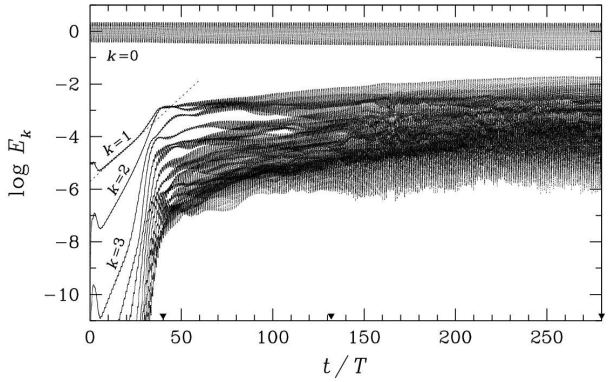

Figure 4: Growth to saturation of the pulsatile inlet flow solution at $U_{red} = 2.5$, $Re = 400$, approximately 3% above Re_c, represented by kinetic energies in azimuthal Fourier modes, with $N_k = 16$. An initial exponential growth phase (indicated by the dotted line) is followed by faster than exponential growth near $t/T \sim 35$, an initial nonlinear saturation at $t/T \approx 40$, then a final slow growth to an asymptotic state, reached at $t/T \sim 250$.

Results

Floquet analysis was carried out at $U_{pm} = 1.75$ and for three values of reduced velocity: $U_{red} = 2.5$, 5, and 7.5, i.e. successively longer dimensionless base flow periods. The corresponding critical Reynolds numbers were found to be $Re_c = 389$, 417 and 500. In all three cases, the instability arose through a period-doubling bifurcation in the $k = 1$ azimuthal Fourier mode. The shape and location of the Floquet instability mode for $U_{red} = 2.5$, $Re = 400$ is shown in figure 3, where it is compared to the base flow at the same instant in time. The alternating sign of the Floquet mode growing on successive base flow pulses for a streamwise traverse at any fixed radius is related to the period-doubling nature of the instability. The perturbation exerts alternating tilting moments on the vortex rings associated with each pulse of the base flow.

Following the stability analysis, full three-dimensional DNS of the instability at $U_{red} = 2.5$, $Re = 400$ was initiated by perturbing the base flow with a small amount of the leading Floquet eigenmode and evolving in time. The time-evolution of energies in the azimuthal modes is shown in figure 4. After a brief equilibration, there is an exponential growth phase in the non-axisymmetric components, lasting until $t/T \approx 35$, following which the perturbation grows faster than exponentially with time before an initial saturation at $t/T \approx 40$, signalling that the bifurcation is subcritical. Then there is an extended slow change until an asymptotic state is approached at $t/T \sim 250$.

The evolution of the flow through time is illustrated by the instantaneous isosurfaces shown in figure 5. The first set of panels, in figure 5 (*a*), shows the flow state after the initial saturation at $t/T = 40$. In the side view, the tilting of the third vortex ring in the view can be seen, while the fourth and fifth rings in the view are further advanced in their breakdowns to a packet of Λ-vortices. In figure 5 (*b*) we see two instances in time leading to the asymptotic state: the slow final growth seen in figure 4 is associated with an upstream movement of the vortex ring breakdown. At $t/T = 280$, the flow still has the symmetry of the Floquet mode, but at that point a small random symmetry-breaking perturbation was added to the first azimuthal mode, and the flow further evolved in time, leading to another asymptotic, but now asymmetric state seen in figure 5 (*c*). At large length and time scales, the flow still has a period-doubling nature, indicating that this is a robust feature.

Discussion

The experimental results of [1, 2, 9] provide a basis for comparison to our DNS results. These were performed at a higher value of U_{red}, but similar Reynolds number ($Re \approx 600$) and peak-to-mean flow ratio ($U_{pm} \approx 1.7$).

In [2] it is stated that 'turbulence was found only for the 75% stenosis and was created only during part of the cycle', whereas in [1] these fluctuations, which are strongest for $2.5 < z/D \leqslant 6$, are characterised as non-turbulent owing to the presence in the conditional velocity spectra of a band of dominant frequencies associated with 'vortex shedding and a turbulent front'. These findings are in quite good agreement with the dye-front flow visualisation and interpretation provided by [9]. For the 75% stenosis, they found four post-stenotic zones: Zone I, reaching to $z/D = 3$, is called the 'stable jet region', although some indication of (apparently axisymmetric) wavy structure can be ob-

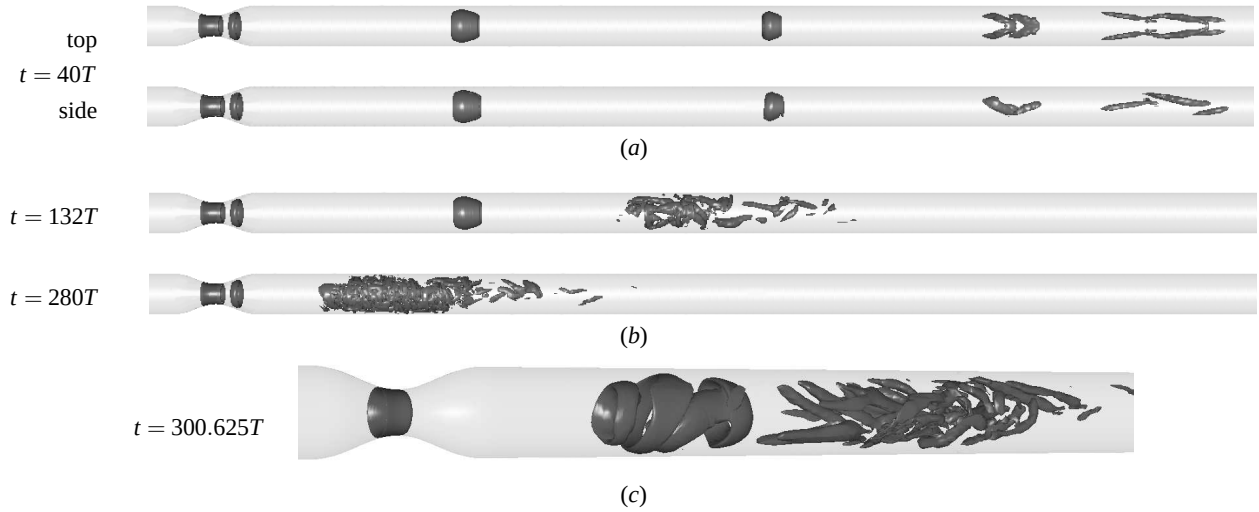

Figure 5: Visualisations for the DNS of pulsatile flow at $U_{red} = 2.5$, $Re = 400$. Isosurfaces are extracted using the λ_2 criterion [8]. (*a*) top and side views of the flow just after the initial saturation seen at $t/T = 40$ in figure 4. (*b*) Two visualisations at later times in the progression to the asymptotic state. Note the upstream movement of breakdown. (*c*) A detail perspective view of the breakdown of vortex rings in the cycle following $t = 300T$. Downstream of the stenosis, the first group of structures shows a ring deforming during the final stages of the tilting process, while the second group shows the decaying breakdown of the previous ring.

served on the jet front in this region; Zone II, $3 < z/D \leqslant 4.5$ is called the 'transition region', where the waves become larger; in Zone III, the 'turbulent region', $4.5 < z/D \leqslant 7.5$, the front rapidly distorts; Zone IV, $z/D > 7.5$ is labelled 'relaminarization'.

These experimental results are thus in reasonable agreement with the kind of asymptotic behaviour we have observed in DNS, as can be seen in figure 5 (*b*, *c*): a rapid distortion of a vortex ring becoming evident a few diameters downstream of the stenosis, leading to a highly unsteady/transitional breakdown at $z/D \sim 6$, following which relaminarisation takes place further downstream.

Conclusions

Floquet analysis of three axisymmetric pulsatile flows shows that they become three-dimensionally unstable through period-doubling bifurcations involving alternating tilting of the vortex rings that are ejected from the stenosis during each pulse cycle. Direct numerical simulation shows that the instability evolves to vortex ring breakdown, which moves progressively upstream until it occurs a comparatively few tube diameters downstream of the stenosis. As the bifurcations are subcritical, hysteretic effects can be expected with respect to changes in Reynolds number, reduced velocity, or peak-to-mean pulsatility near the onset of three-dimensionality. The breakdowns are energetic turbulent events, and will lead to regions of high temporal and spatial gradients of wall shear stress where they occur. For the Reynolds numbers studied here, the flow relaminarises further downstream, and will eventually recover the conditions of the pulsatile inflow. These findings are in good agreement with available experimental results.

Acknowledgements

This work was supported by the Australian Partnership for Advanced Computing, the Royal Academy of Engineering, and the UK Engineering and Physical Sciences Research Council.

References

[1] Ahmed SA. An experimental investigation of pulsatile flow through a smooth constriction. *Exptl Thermal & Fluid Sci*, **17**: 309–318, 1998

[2] Ahmed SA & Giddens DP. Pulsatile poststenotic flow studies with laser Doppler anemometry. *J Biomechanics*, **17**(9): 695–705, 1984

[3] Barkley D & Henderson RD. Three-dimensional Floquet stability analysis of the wake of a circular cylinder. *J Fluid Mech*, **322**: 215–241, 1996

[4] Berger SA & Jou LD. Flows in stenotic vessels. *Annu Rev Fluid Mech*, **32**: 347–384, 2000

[5] Blackburn HM. Three-dimensional instability and state selection in an oscillatory axisymmetric swirling flow. *Phys Fluids*, **14**(11): 3983–3996, 2002

[6] Blackburn HM & Lopez JM. The onset of three-dimensional standing and modulated travelling waves in a periodically driven cavity flow. *J Fluid Mech*, **497**: 289–317, 2003

[7] Blackburn HM & Sherwin SJ. Formulation of a Galerkin spectral element–Fourier method for three-dimensional incompressible flows in cylindrical geometries. *J Comput Phys*, **197**(2): 759–778, 2004

[8] Jeong J & Hussain F. On the identification of a vortex. *J Fluid Mech*, **285**: 69–94, 1995

[9] Ojha M, Cobbold RSC, Johnston KW & Hummel RL. Pulsatile flow through constricted tubes: An experimental investigation using photochromic tracer methods. *J Fluid Mech*, **203**: 173–197, 1989

[10] Tuckerman LS & Barkley D. Bifurcation analysis for timesteppers. In E Doedel & LS Tuckerman, editors, *Numerical Methods for Bifurcation Problems and Large-Scale Dynamical Systems*, 453–566. Springer, 2000